Received: 29 October 2021 | Revised: 17 January 2022 | Accepted: 20 January 2022

DOI: 10.1002/jcc.26817

RESEARCH ARTICLE

Journal of COMPUTATIONAL CHEMISTRY WILEY

Formation and infrared spectroscopic characterization of carbon suboxide complexes TM-η^1-C_3O_2 and the inserted ketenylidene complexes OCTMCCO (TM=Cu, Ag, Au) in solid neon

Hongmin Li | Yangyu Zhou | Guanjun Wang | Xiaoqing Zeng | Mingfei Zhou

Department of Chemistry, Shanghai Key Laboratory of Molecular Catalysis and Innovative Materials, Fudan University, Shanghai, China

Correspondence
Mingfei Zhou, Department of Chemistry, Shanghai Key Laboratory of Molecular Catalysis and Innovative Materials, Fudan University, Shanghai 200438, China.
Email: mfzhou@fudan.edu.cn

Funding information
China Postdoctoral Science Foundation, Grant/Award Number: 2020M681148; National Natural Science Foundation of China, Grant/Award Number: 21688102

Abstract

The reactions of coinage metal atoms Cu, Ag and Au with carbon suboxide (C_3O_2) are studied by matrix isolation infrared spectroscopy. The weakly bound complexes TM-η^1-C_3O_2 (TM=Cu, Ag, Au), in which the carbon suboxide ligand binds to the metal center in the monohapto fashion are formed as initial reaction products. The complexes subsequently isomerize to the inserted products OCTMCCO upon visible light (λ = 400–500 nm) excitation. The analysis of the electronic structure using modern quantum chemistry methods suggests that the linear OCTMCCO complexes are best described by the bonding interactions between the TM^+ cation in the electronic singlet ground state and the $[OC...CCO]^-$ ligands in the doublet state forming two $TM^+ \leftarrow$ ligands σ donation and two $TM^+ \rightarrow$ ligands π backdonation bonding components. In addition, the CuCCO, AgCCO and AuCCO complexes are also formed, which are predicted to be bent.

KEYWORDS
carbon suboxide, IR spectroscopy, ketenylidene complexes, matrix isolation, quantum chemical calculations

1 | INTRODUCTION

Carbon suboxide (C_3O_2) is a stable dioxide of carbon, which was conventionally described as a linear cumulene O=C=C=C=O based on early spectroscopic and electron diffraction investigations.[1–6] However, later high-resolution infrared spectroscopic and ab initio theoretical studies confirmed that the molecule is bent in the gas phase with a very flat bending potential.[7–9] The observation of a bent equilibrium geometry indicates that the bonding of carbon suboxide cannot be interpreted using the cumulenic electron-sharing bonding model. It is better described using the donor-acceptor bonding model. The ground-state of bent C_3O_2 molecule can be classified as a dicarbonyl complex of carbon in its ^1D excited state with a valence electron configuration $(2s)^0 (2p_\sigma)^2 (2p_{\pi\|})^0 (2p_{\pi\perp})^2$.[10,11] The C_3O_2 molecule is a divalent carbon (0) complex with the central carbon atom possessing two lone pairs of electrons. Thus, C_3O_2 acts as a strong Lewis base, which was determined to have a negative electron affinity and a quite large proton affinity.[12–17]

Although carbon suboxide is widely used as a reactant in synthetic chemistry,[18] its coordination chemistry as a Lewis base and subsequent metal mediated activation have received very little attention. Stable carbon suboxide complexes of transition metals Ni, Pd, and Pt supported by ligands such as phosphines and halides were synthesized.[19–21] Solid-state IR and NMR spectroscopic as well as theoretical studies indicate that the carbon suboxide ligand is bound to the metal center in an η^2-fashion through two carbon atoms.[22,23] Theoretical studies suggest that C_3O_2 binds one AuCl preferentially in the η^1 mode, whereas the η^1- and η^2-bonded modes are energetically nearly degenerate in the diaurated complex.[24] Infrared photodissociation spectroscopic investigation on the $[TM(CO)_4(C_3O_2)]^+$ (TM=Fe,

Co, Ni) complexes shows that the C_3O_2 ligand binds to the metal center in the η^1 fashion.[25] Very recently, it was found that a dinuclear titanium complex reacted with carbon suboxide forming an adduct, which was structurally authenticated to involve an η^2-corodinated C_3O_2 ligand.[26] The C_3O_2 adduct further reacted with additional two C_3O_2 molecules resulting in trimerization of the C_3O_2 molecules. The activation of C_3O_2 by a U(III) complex via the reductive coupling of three C_3O_2 molecules in forming a tetranuclear complex with concomitant loss of CO was also reported.[27] The reaction is proceeded via the formation of a dimeric bridging ketene complex intermediate, which undergoes insertion of C_3O_2 to form the final product.

In this paper, we report a combined matrix isolation spectroscopic and theoretical study on the reactions of coinage metal atoms copper, silver, and gold with carbon suboxide in solid neon. We will show that the reactions proceed with the initial formation of the weakly bound complexes TM-η^1-C_3O_2 (TM=Cu, Ag, Au), in which the carbon suboxide ligand binds to the metal center in the monohapto fashion. The complexes can further isomerize to the inserted products OCTMCCO upon visible light (λ = 400–500 nm) excitation.

2 | METHODS

2.1 | Experimental method

The experimental method for matrix isolation infrared spectroscopy has been described in detail previously.[28] In short, the Nd:YAG laser fundamental (Continuum Minilite II; 10 Hz repetition rate with 10 ns pulse width) was used to ablate rotating metal target to produce metal atoms. The laser-ablated metal atoms were co-deposited with carbon suboxide (0.05%) in excess neon onto a 4 K CsI window, which was cooled by means of a closed-cycle helium refrigerator. The C_3O_2 sample was synthesized according to published protocols[29] by the reaction of malonic acid and P_2O_5 at 140°C. The volatile products were directed through three cold U-traps held at −110, −145, and −196°C, and pure C_3O_2 was collected in the middle trap. The purity of C_3O_2 was checked by gas-phase IR spectroscopy. The isotopic substituted OC^{13}CCO sample was prepared and purified in the same way as OCCCO, with the ^{13}C substitute of malonic acid (2-^{13}C, 99.0%, Cambridge Isotope Laboratories, Inc.). After 0.5 h of sample deposition, infrared absorption spectrum in the mid-infrared region (4000–450 cm^{-1}) was recorded at 0.5 cm^{-1} resolution on a Bruker 80 V spectrometer using a liquid nitrogen cooled HgCdTe (MCT) detector. Matrix samples were annealed at different temperatures and quickly cooled back to 4 K for spectral detection. Selected samples were subjected to photolysis using a high-pressure mercury arc lamp (250 W, 250–580 nm) with the outer globe removed.

2.2 | Theoretical method

Density functional theory (DFT) calculations were performed to predict the molecular structures and to verify the assignments of vibrational frequencies of the observed species. The geometry optimization and harmonic vibrational frequency calculations were carried out with the Gaussian 09 package[30] at the level of three parameter hybrid functional B3LYP.[31–33] Dunning's correction consistent basis set with the polarized triple-ζ plus diffuse functions aug-cc-pVTZ[34] was used for the C and O atoms, and the SDD pseudopotential and basis set[35] was used for the Cu, Ag and Au atoms. Considering the weak interaction between the metal atom and the C_3O_2 molecule, the D3 correction[36] was used for the calculations. In order to identify the bonding situation in the OCTMCCO complexes, an energy decomposition analysis (EDA)[37] in conjunction with the natural orbitals for chemical valence (NOCV)[38] method was performed at the PBE/TZ2P//B3LYP/aug-cc-pVTZ level of theory.[39] The EDA-NOCV calculations were carried out using the ADF 2014.10 program package.[40,41]

3 | RESULTS AND DISCUSSION

3.1 | Infrared spectra

The infrared spectra in selected regions from co-deposition of laser-ablated Cu, Ag, and Au atoms with C_3O_2 molecules in excess neon are shown in Figures 1–3, respectively. The stepwise annealing and photolysis behavior of the product absorptions are also shown in the figures. Absorptions common to these experiments at 2075.7, 1975.4, 1738.1, 1403.0, 1069.3 and 811.5 cm^{-1} were observed. The 2075.7, 1738.1, 1403.0 and 811.5 cm^{-1} absorptions have been assigned to the $C_3O_2^-$ anion.[17] These absorptions were presented after sample deposition at 4 K, decreased on annealing and disappeared under blue light (440 ± 20 nm) irradiation. The absorptions at 1975.4 and

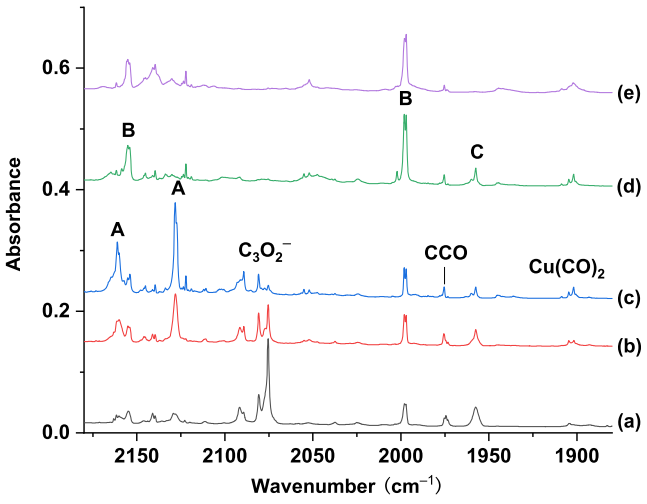

FIGURE 1 Infrared spectra in the 2180–1880 cm^{-1} region from co-deposition of laser-ablated Cu atoms with 0.05% C_3O_2 in neon. (A) After 30 min of sample deposition, (B) after annealing to 10 K, (C) after annealing to 12 K, (D) after 10 min of blue light irradiation, and (E) after 10 min of UV–visible light irradiation. **A**: Cu-η^1-C_3O_2; **B**: OCCuCCO; **C**: CuCCO

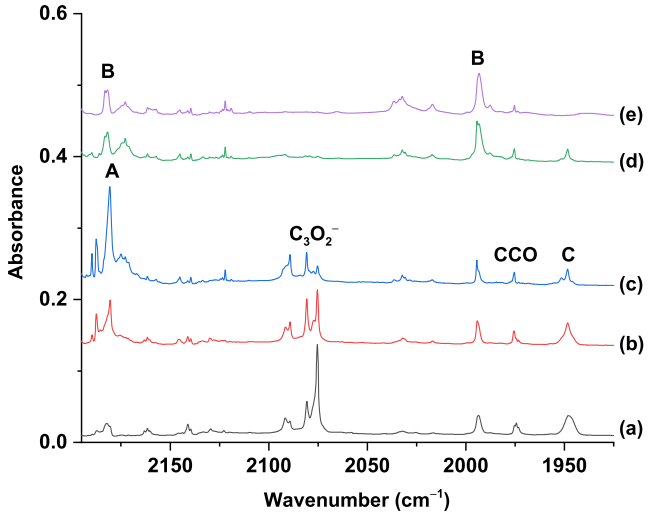

FIGURE 2 Infrared spectra in the 2195–1925 cm^{-1} region from co-deposition of laser-ablated Ag atoms with 0.05% C_3O_2 in neon. (A) After 30 min of sample deposition, (B) after annealing to 10 K, (C) after annealing to 12 K, (D) after 10 min of blue light irradiation, and (E) after 10 min of UV–visible light irradiation. **A**: Ag-η^1-C_3O_2; **B**: OCAgCCO; **C**: AgCCO

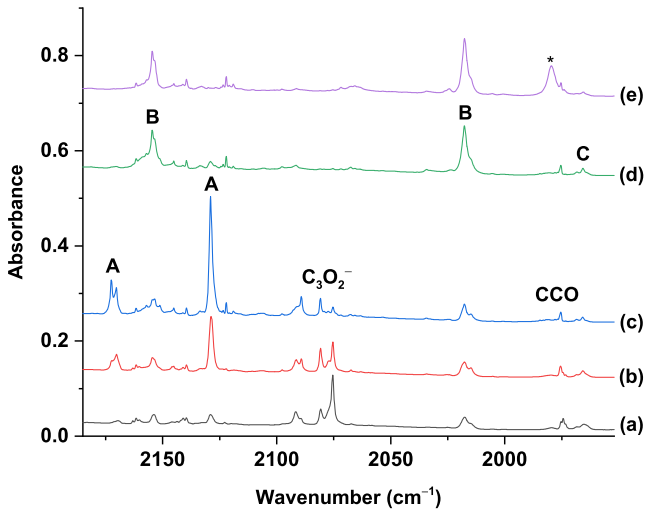

FIGURE 3 Infrared spectra in the 2185–1952 cm^{-1} region from co-deposition of laser-ablated Au atoms with 0.05% C_3O_2 in neon. (A) After 30 min of sample deposition, (B) after annealing to 10 K, (C) after annealing to 12 K, (D) after 10 min of blue light irradiation, and (E) after 10 min of 580 nm > λ > 280 nm UV–visible light irradiation. **A**: Au-η^1- C_3O_2; **B**: OCAuCCO; **C**: AuCCO

1069.3 cm^{-1} are attributed to CCO, which were observed at 1987 and 1077 cm^{-1} in solid N_2 matrix and at 1969 and 1064 cm^{-1} in solid argon matrix.[29,42] Besides these common absorptions, metal dependent absorptions from the reactions of metal atoms with C_3O_2 molecules were also observed, which can be divided into several groups based on their behaviors on sample annealing and photolysis (labeled as A–C in Figures 1–3). In the case of copper, absorptions at 1904.6 and 1901.9 cm^{-1} can be assigned to the copper dicarbonyl complex.[43]

Experiments were also performed using the central carbon isotopically labeled sample OC^{13}CCO and the OCCCO + OC^{13}CCO mixture. The spectra in selected regions are shown in Figures S1–S6, respectively.

3.2 | TM-η^1-C_3O_2

The absorptions labeled as **A** in each spectrum are assigned to the TM-η^1-C_3O_2 complexes. These absorptions are observed as weak bands after sample deposition, increase tremendously when the samples are annealed to 10 K and 12 K, but are completely depleted under 10 min of blue light irradiation. Two bands at 2160.7 and 2128.2 cm^{-1} are assigned to the Cu-η^1-C_3O_2 complex. Both bands are red-shifted by more than 100 cm^{-1} from the antisymmetric CO stretching mode of C_3O_2. In the experiment with the OC^{13}CCO sample, the bands shift to 2159.3 and 2116.9 cm^{-1} with ^{13}C isotopic shift of 1.4 and 11.3 cm^{-1}, respectively. No intermediate absorptions are observed in the experiment using the 1:1 molar mixture of OCCCO and OC^{13}CCO, confirming that only one C_3O_2 ligand is involved in the complex. The low mode shows larger isotopic shift than the upper mode when the central carbon atom is isotopic substituted, implying more central carbon atom involvement in the vibration of the low mode. Accordingly, the 2128.2 cm^{-1} band is assigned to the antisymmetric CO stretching mode, while the 2160.7 cm^{-1} band is attributed to the symmetric stretching mode. The assignment is strongly supported by DFT calculations. As listed in Table 1, the two experimentally observed modes are predicted at 2219.7 and 2196.6 cm^{-1} with ^{13}C isotopic shifts of 1.5 and 10.3 cm^{-1}, respectively, both of which match the observed values very well. As shown in Figure 4, the Cu-η^1-C_3O_2 complex is predicted to have an $^2A_1$ electronic ground state with planar C_{2v} symmetry. The complex is predicted to have a Cu–C bond distance of 2.044 Å, longer than that of CuCO (1.969 Å) calculated at the same level.[43]

Only the antisymmetric CO stretching mode is observed at 2181.0 cm^{-1} for the Ag-η^1-C_3O_2 complex. The absorptions at 2189.8 and 2187.5 cm^{-1} are due to site absorptions. The 2181.0 cm^{-1} absorption shifts to 2166.0 cm^{-1} with the OC^{13}CCO sample. The isotopic shift of 15.0 cm^{-1} indicates that it is an antisymmetric stretching mode. The symmetric stretching mode is not observed in the experiments. The B3LYP-D3 calculations indicate that Ag-η^1-C_3O_2 is a weakly bound van der Waals complex. It is predicted to have a quite long Ag–C distance of 2.826 Å, which is significantly longer than the Ag—C bond length (2.3 Å) observed for Ag_2CCO,[44] and is much longer than the sum of the single bond covalent radii of Ag and C atoms (2.03 Å).[45] The binding energy with respect to the ground state Ag atom and C_3O_2 is predicted to be only 1.0 kcal mol^{-1}. The antisymmetric stretching mode is predicted at 2311.8 cm^{-1} with a ^{13}C isotopic shift of 22.2 cm^{-1}. The symmetric stretching mode is predicted at 2249.3 cm^{-1} with IR intensity only about one eighth of the antisymmetric stretching mode and cannot be observed experimentally.

The Au-η^1-C_3O_2 complex is observed to absorb at 2171.6 and 2129.0 cm^{-1}. The band positions and isotopic frequency shifts (1.3 and 10.3 cm^{-1}) are very close to those of the Cu-η^1-C_3O_2 complex,

TABLE 1 Experimental and calculated vibrational frequencies (cm^{-1}) and isotopic frequency shifts (cm^{-1}) of the TM-η^1-C_3O_2 (TM=Cu, Ag, Au) complexes

Exptl.		Calcd.		
Cu-η^1-C_3O_2				
ν[a]	$\Delta\nu$[b]	ν[c]	$\Delta\nu$[d]	Assignment[e]
2160.7	1.4	2219.7 (768)	1.5	C-O sym. str. (a_1)
2128.2	11.3	2196.6 (1836)	10.3	C-O asym. str. (b_2)
		1430.0 (<1)	37.4	C-C str. (b_2)
		927.0 (83)	16.7	CCC bend. (a_1)
		579.9 (29)	6.6	OCCCO wag. (b_1)
		574.3 (0)	0.0	OC wag. (a_2)
		533.0 (58)	1.7	CCC scissor. (a_1)
		468.8 (43)	0.1	CCC rock. (b_2)
		237.9 (6)	3.0	Cu-C str. (a_1)
		143.3 (1)	3.5	OCCCO wag. (b_1)
		104.9 (6)	0.1	OCCCO scissor. (a_1)
		85.4 (<1)	2.4	OCCCO rock. (b_2)
Ag-η^1-C_3O_2				
2181.0	15.0	2311.8 (2307)	22.2	C-O asym. str. (b_2)
		2249.3 (305)	0.4	C-O sym. str. (a_1)
		1597.8 (24)	35.6	C-C str. (b_2)
		857.5 (12)	8.0	CCC bend. (a_1)
		586.8 (<1)	0.0	O-C wag. (a_2)
		569.1 (33)	5.2	OCCCO wag. (b_1)
		565.6 (6)	0.1	CCC rock. (b_2)
		564.2 (23)	2.5	CCC scissor. (a_1)
		87.6 (<1)	2.3	OCCCO wag. (b_1)
		78.9 (2)	1.1	OCCCO scissor. (a_1)
		58.3 (4)	0.5	Ag-C str. (a_1)
		39.8 (<1)	0.1	OCCCO rock. (b_2)
Au-η^1-C_3O_2				
2171.6	1.3	2231.8 (728)	1.3	C-O sym. str. (a_1)
2129.0	10.3	2210.4 (1877)	10.7	C-O asym. str. (b_2)
		1457.1 (<1)	38.0	C-C str. (b_2)
		931.6 (16)	16.8	CCC bend. (a_1)
		585.2 (28)	6.6	OCCCO wag. (b_1)
		574.5 (0)	0.0	OC wag. (a_2)
		559.4 (4)	1.8	CCC scissor. (a_1)
		512.0 (24)	0.1	CCC rock. (b_2)
		218.3 (4)	3.5	Au-C str. (a_1)
		144.0 (1)	3.4	OCCCO wag. (b_1)
		100.2 (2)	0	OCCCO scissor. (a_1)
		85.1 (<1)	0.4	OCCCO rock. (b_2)

[a]Observed IR band positions in neon matrix at 4 K.
[b]Observed $^{12/13}C$ isotopic shifts.
[c]The calculated IR intensities are listed in parentheses in km mol^{-1} at the B3LYP-D3/aug-cc-pVTZ/SDD level.
[d]Calculated $^{12/13}C$ isotopic shifts.
[e]Tentative assignments based on calculated vibrational displacement vectors.

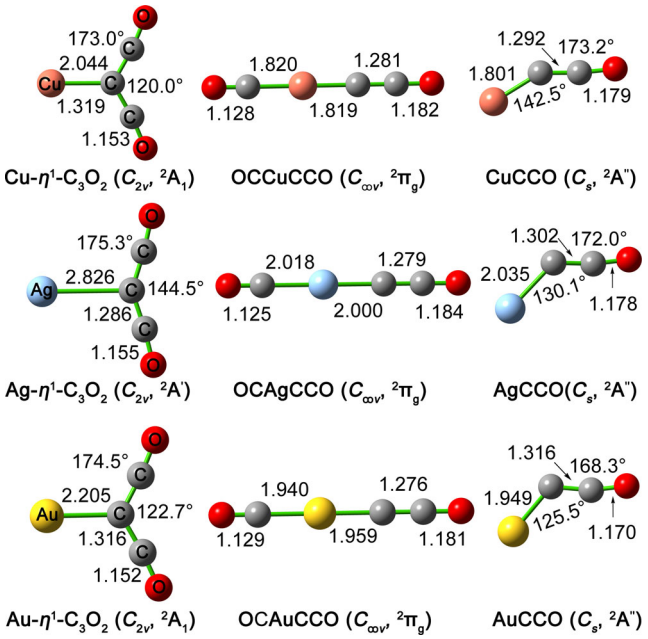

FIGURE 4 Optimized structures (bond lengths in angstroms and bond angles in degrees) of TM-η^1-C_3O_2, OCTMCCO and TMCCO (TM=Cu, Ag, Au) at the B3LYP-D3 level

suggesting similar bonding situation between copper and gold. The complex is also predicted to have a planar C_{2v} structure (Figure 4) with an Au–C bond distance of 2.205 Å, which is very close to that of 2.217 Å in $Au(CO)_4^+$.[46] As listed in Table 1, the calculated stretching frequencies and isotopic shifts are in excellent agreement with the experimental values.

The binding energies of the TM-η^1-C_3O_2 complexes with respect to the ground state metal atoms and C_3O_2 molecule are estimated to be 6.9, 1.0 and 6.8 kcal mol^{-1} with TM=Cu, Ag and Au, respectively (Table 2). The binding energies of the three metals show the usual V-shaped trend in which the third transition-metal-row atom Au exhibits stronger interaction than the second-row metal Ag due to relativistic effects. Similar situation has been reported and discussed for the coinage metal monocarbonyl complexes.[47–49]

3.3 | OCTMCCO

Besides the TM-η^1-C_3O_2 absorptions, a second group of absorptions labeled as **B** in each spectrum are observed after sample deposition. These absorptions remain almost unchanged upon sample annealing, but increase about three fold under blue light irradiation at the expense of the TM-η^1-C_3O_2 complex absorptions. The photochemical behavior implies that species **B** is a structural isomer of species **A**, and is assigned to the OCTMCCO complexes. In the case of copper, two absorptions at 2154.8 and 1997.5 cm^{-1} are observed. The upper band shows only 0.1 cm^{-1} shift with the $OC^{13}CCO$ sample. The band position and isotopic shift are appropriate for a terminally bonded carbonyl stretching vibration. The band position is slightly blue-shifted

TABLE 2 Calculated reaction energies (kcal mol^{-1}) for the TM + C_3O_2 reactions at the B3LYP level

Cu + C_3O_2 → Cu-η^1-C_3O_2	−6.9
Ag + C_3O_2 → Ag-η^1-C_3O_2	−1.0
Au + C_3O_2 → Au-η^1-C_3O_2	−6.8
Cu-η^1-C_3O_2 → OCCuCCO	−3.6
Ag-η^1-C_3O_2 → OCAgCCO	+16.8
Au-η^1-C_3O_2 → OCAuCCO	+0.3
OCCuCCO → CuCCO + CO	+35.4
OCAgCCO → AgCCO + CO	+25.2
OCAuCCO → AuCCO + CO	+40.1
Cu + CCO → CuCCO	−66.9
Ag + CCO → AgCCO	−50.9
Au + CCO → AuCCO	−58.2

from that of free CO (2140.8 cm^{-1} in Ne), suggesting that the carbonyl ligand is coordinated to a positively charged metal center. The low band is attributed to the CO stretching mode of a CCO subunit, which is about 22.1 cm^{-1} higher than that of free CCO in solid Ne matrix. It shifts to 1986.6 cm^{-1} with a carbon-13 isotopic shift of 10.9 cm^{-1} when the OC^{13}CCO sample is used. The spectrum from the experiment with the OCCCO + OC^{13}CCO mixed sample confirms the involvement of only one CCO unit. The OCCuCCO assignment is further supported by B3LYP calculations. The complex is predicted to have a linear structure and a $^2\Pi_g$ ground state, which is 3.6 kcal mol^{-1} lower in energy than the Cu-η^1-C_3O_2 complex isomer. The two Cu-C bond lengths of OCCuCCO are predicted to be 1.820 and 1.819 Å, respectively, which are very close to that of 1.835 Å in $Cu(CO)_2$.[43] Note that these Cu-C bond length values are about the same as the sum of the double-bond covalent radii of Cu and C atoms (1.82 Å),[50] suggesting some multiple bonding character. As listed in Table 3, the two experimentally observed modes are predicted at 2200.4 and 2053.6 cm^{-1} with the ^{13}C isotopic shifts of 0.1 and 10.9 cm^{-1}, which match the observed values very well. The other modes are predicted to have very low IR intensities, and cannot be observed experimentally.

The 2182.4 and 1993.3 cm^{-1} bands in the Ag+C_3O_2 experiments are assigned to the OCAgCCO molecule. The OCAg^{13}CCO isotopomer is observed at 2182.2 and 1982.9 cm^{-1}. The OCAgCCO molecule is calculated to have a linear structure with OC-Ag and Ag-CCO bond distances of 2.018 and 2.000 Å, very close to the sum of the double-bond covalent radii of Ag and C atoms (2.06 Å).[50] This isomer is predicted to be higher in energy than the Ag-η^1-C_3O_2 complex by 16.8 kcal mol^{-1} at the B3LYP level of theory. The two CO stretching vibrational modes are calculated at 2213.0 and 2048.2 cm^{-1} with ^{13}C isotopic shifts of 0.1 and 11.5 cm^{-1}, respectively.

Analogous bands at 2154.1 and 2017.7 cm^{-1} in the Au + C_3O_2 experiments are assigned to the OCAuCCO molecule. The OC^{13}CCO counterparts are observed at 2153.9 and 2005.4 cm^{-1} with isotopic shifts of 0.2 and 12.3 cm^{-1}. Calculations predict that the OCAuCCO molecule is also linear, and is less stable than the Au-η^1-C_3O_2 isomer by 0.3 kcal mol^{-1} at the B3LYP level. The two experimentally

TABLE 3 Experimental and calculated vibrational frequencies (cm^{-1}) and isotopic shifts (cm^{-1}) of the OCTMCCO (TM=Cu, Ag, Au) complexes

Exptl.		Calcd.		
OCCuCCO				
ν[a]	$\Delta\nu$[b]	ν[c]	$\Delta\nu$[d]	Assignment[e]
2154.8	0.1	2200.4 (685)	0.1	O-C str.
1997.5	10.9	2053.6 (1379)	10.9	CC-O str.
		1379.2 (4)	34.3	C-CO str.
		551.7 (14)	4.8	CCO bend.
		540.5 (5)	2.7	CCO bend.
		462.2 (2)	0.4	OC-Cu str.
		392.6 (1)	0.4	O-C rock.
		374.2 (1)	0.3	O-C wag.
		350.9 (35)	1.6	Cu-CCO str.
		163.6 (5)	3.9	OCCuCCO bend.
		130.8 (9)	3.2	OCCuCCO bend.
		47.7 (1)	0	OCCuCCO wag.
		41.6 (<1)	0.1	OCCuCCO rock.
OCAgCCO				
2182.4	0.2	2213.0 (649)	0.1	O-C str.
1993.3	10.4	2048.2 (1353)	11.5	CC-O str.
		1367.2 (4)	33.3	C-CO str.
		539.4 (14)	4.2	CCO bend.
		530.4 (4)	2.4	CCO bend.
		375.4 (<1)	1.0	OC-Ag str.
		330.6 (1)	0.3	O-C rock.
		315.0 (<1)	0.4	O-C wag.
		309.4 (41)	1.6	Ag-CCO str.
		141.3 (4)	3.6	OCAgCCO bend.
		101.9 (7)	2.5	OCAgCCO bend.
		41.9 (<1)	0	OCAgCCO wag.
		25.9 (<1)	0.1	OCAgCCO rock.
OCAuCCO				
2154.1	0.2	2194.4 (683)	0.3	O-C str.
2017.7	12.3	2072.6 (1582)	12.2	CC-O str.
		1401.5 (6)	34.5	C-CO str.
		545.6 (9)	4.9	CCO bend.
		522.7 (7)	2.0	CCO bend.
		442.1 (3)	0.8	OC-Au str.
		422.3 (5)	0.4	O-C rock.
		422.2 (27)	0	O-C wag.
		368.3 (15)	2.6	Au-CCO str.
		171.1 (1)	4.3	OCAuCCO bend.
		131.1 (4)	3.4	OCAuCCO bend.
		49.2 (<1)	0	OCAuCCO wag.
		32.0 (<1)	0.2	OCAuCCO rock.

[a]Observed IR band positions in neon matrix at 4 K.
[b]Observed $^{12/13}$C isotopic shifts.
[c]The calculated IR intensities are listed in parentheses in km mol^{-1} at the B3LYP-D3/aug-cc-pVTZ/SDD level.
[d]Calculated $^{12/13}$C isotopic shifts.
[e]Tentative assignments based on calculated vibrational displacement vectors.

observed modes are simulated at 2194.4 and 2072.6 cm^{-1} possessing the ^{13}C isotopic shifts of 0.3 and 12.2 cm^{-1}, in excellent agreement with the experimental values. As shown in Figure 4, the OCAuCCO molecule is predicted to have OC-Au and Au-CCO bond lengths of 1.940 and 1.959 Å, shorter than the sum of the single-bond atomic radii of Au and C (1.99 Å)[45] but longer than the sum of the double-bond atomic radii of Au and C (1.88 Å).[50]

3.4 | TMCCO

The 1957.5 cm^{-1} band (labeled as **C**) in the Cu + C_3O_2 experiments is presented after sample deposition, decreases upon annealing to 12 K, increases on visible-light irradiation, but disappears completely under subsequent UV–visible light irradiation (Figure 1). It shifts to 1951.0 cm^{-1} with $OC^{13}CCO$, giving an isotopic shift of 6.5 cm^{-1}. The band position and isotopic shift suggest the assignment to the CC-O stretching vibration of a CuCCO complex. The experiment using the OCCCO + $OC^{13}CCO$ mixture sample confirms the involvement of one CCO subunit. The CuCCO molecule is predicted to have a $^2A''$ ground state with C_s symmetry. The molecule is bent with a ∠CuCC bond angle of 142.5°. The linear structure is less stable than the bent structure by only 0.3 kcal mol^{-1}. The Cu—C bond distance is predicted to be 1.801 Å, slightly shorter than the Cu═C double bond distance (1.82 Å).[50] The CC—O stretching mode of bent CuCCO is calculated at 2033.3 cm^{-1} (Table 4). The C—CO stretching mode is computed at 1328.5 cm^{-1} with very low IR intensity and is not observed experimentally.

TABLE 4 Experimental and calculated vibrational frequencies (cm^{-1}) and isotopic shifts (cm^{-1}) of the TMCCO (TM═Cu, Ag, Au) complexes

Exptl.		Calcd.		
CuCCO				
ν[a]	$\Delta\nu$[b]	ν[c]	$\Delta\nu$[d]	Assignment[e]
1957.5	6.5	2033.3 (751)	8.3	CC-O str. (a')
		1328.5 (6)	33.9	C-CO str. (a')
		554.3 (11)	6.2	CCO bend. (a')
		455.0 (15)	1.6	CCO bend. (a'')
		438.9 (4)	3.4	Cu-C str. (a')
		64.1 (21)	1.2	CuCC scissor. (a')
AgCCO				
1947.3	7.3	1999.4 (850)	6.1	CC-O str. (a')
		1267.7 (4)	32.4	C-CO str. (a')
		568.9 (14)	6.5	CCO bend. (a')
		450.5 (16)	1.8	CCO bend. (a'')
		384.3 (4)	6.1	Ag-C str. (a')
		81.1 (14)	1.2	AgCC scissor. (a')
AuCCO				
1965.9	4.2	2018.4 (877)	4.1	CC-O str. (a')
		1246.2 (4)	33.8	C-CO str. (a')
		608.9 (28)	11.0	CCO bend. (a')
		433.5 (<1)	4.9	Au-C str. (a')
		429.3 (16)	1.4	CCO bend. (a'')
		104.8 (11)	1.4	AuCC scissor. (a')

[a]Observed IR band positions in neon matrix at 4 K.
[b]Observed $^{12/13}C$ isotopic shifts.
[c]The calculated IR intensities are listed in parentheses in km mol^{-1} at the B3LYP-D3/aug-cc-pVTZ/SDD level.
[d]Calculated $^{12/13}C$ isotopic shifts.
[e]Tentative assignments based on calculated vibrational displacement vectors.

Similar bands at 1947.3 and 1940.0 cm^{-1} in the Ag experiments are assigned to the C—O stretching modes of the AgCCO and $Ag^{13}CCO$ complexes. DFT calculations predict that the AgCCO complex also has a $^2A''$ ground state and a bent C_s symmetric structure with a ∠AgCC angle of 130.1°. The linear structure is 1.2 kcal mol^{-1} higher in energy than the bent structure. The observed vibrational mode is predicted at 1999.4 and 1993.3 cm^{-1} for the AgCCO and $Ag^{13}CCO$ isotopomers, which match the experimental values very well.

Similar band at 1965.9 cm^{-1} in the Au + C_3O_2 experiments is assigned to the AuCCO complex. It shifts to 1961.7 cm^{-1} with the $OC^{13}CCO$ sample. The AuCCO complex is predicted to have a bent structure with an Au—C bond distance of 1.949 Å, which is slightly longer than the Au═C double bond distance (1.88 Å).[50] The C-O stretching mode is predicted at 2018.4 cm^{-1} with an isotopic shift of 4.1 cm^{-1}, in excellent with the observed values.

3.5 | Bonding analysis

The calculated atomic partial charges and spin densities of the TM-η^1-C_3O_2 complexes are shown in Figure S7. The spin density of the Ag-η^1-C_3O_2 complex is almost entirely located on the metal center. The calculated binding energy (1 kcal mol^{-1}) is much lower than those of Cu-η^1-C_3O_2 and Au-η^1-C_3O_2 (6.8 and 6.9 kcal mol^{-1}), suggesting that the Ag-η^1-C_3O_2 is a weakly bound van der Waals complex, which is supported by the noncovalent interaction (NCI) analysis as shown in Figure S8.

The highest-lying molecular orbitals of the doublet ground state OCTMCCO complexes are shown in Figure 5. The unpaired electron occupies a molecular orbital which is primarily a π symmetry MO of the CCO unit that is C-C bonding but C—O antibonding in character. The HOMO-1 and HOMO-2 are metal d_σ and d_δ orbitals. The HOMO-3 are doubly degenerate metal d_π orbitals that comprise weak metal to ligands π backdonation. The HOMO-4 is a ligand-based orbital that comprises some ligands to metal σ donation. The analysis using the adaptive natural density partitioning (AdNDP) method[51] on OCAuCCO shows that there are two 2c-2e Au-C σ bonds, one 6c-2e delocalized π bond and one 6c-1e delocalized π bond (Figure S9), suggesting some Au-C multiple bonding character. Mulliken population analysis shows that the spin density is mainly located on the CCO moiety (Figure S10). The metal centers are positively charged

(Table S1). Therefore, the doublet ground state of OCTMCCO can be regarded as involving bonding interaction between a TM^+ cation in the electronic singlet ground state ^1S and the $[OC...CCO]^-$ ligands in the doublet state with the unpaired electron in the π orbital of CCO^-. The bonding between the metal cation and the $[OC...CCO]^-$ ligand anion in the OCTMCCO complexes is analyzed with the EDA-NOCV method, which can provide a quantitative evaluation of the strength of bonding. Table 5 shows the numerical results which give the strength of the different orbital interactions. The results show that the strength of the interaction energy ΔE_{int} of the three metals shows the usual V-shaped trend in which the third-row transition metal Au exhibits the strongest interactions whereas the second-row metal Ag has the weakest interactions. The attractive metal–ligand interactions in all three complexes come mainly from Coulomb attraction, which contributes 71.4% for TM=Cu, 73.7% for TM=Ag, and 69.5% for TM=Au of the binding forces. The much stronger bonding in OCAuCCO can be attributed to the much bigger orbital interactions than those in OCCuCCO and OCAgCCO due to relativistic effects. Further inspection of the orbital components shows that there are four relatively strong orbital interaction terms $\Delta E_{orb\ (1)}$–$\Delta E_{orb\ (4)}$ that can be identified with specific σ or π dative interactions with the help of the associated deformation densities $\Delta\rho_{\ (1)}$–$\Delta\rho_{\ (4)}$ displayed in Figure 6 or Figures S11–S13, which illustrate well the charge flow that accompanies the orbital terms. For each complex, there are two components for the donation of the occupied ligand MOs to TM^+ and two components for the π-backdonation of the occupied AOs of TM^+ to ligands. The strongest orbital stabilization $\Delta E_{orb\ (1)}$ is due to the σ-donation of the +,+ combination of the ligand HOMO and HOMO-1 MOs into the corresponding vacant LUMOs AO of TM^+, followed by the σ-donation $\Delta E_{orb\ (2)}$ of the +,− combination of the lone-pair HOMO and HOMO-1 MOs of ligands into the vacant LUMO+1 p_z AO of TM^+. The two relatively weak orbital contributions $\Delta E_{orb\ (3)}$ and $\Delta E_{orb\ (4)}$ come from the $\pi_{||}$- and $\pi_{\perp}$-backdonation of the occupied d_{yz} and d_{xz} AOs of the TM^+ into the two orthogonal LUMO MOs of the ligands. The $\Delta E_{orb\ (1)}$ term of the OCAuCCO complex is about twice as large as those of OCCuCCO and OCAgCCO due to low-lying nature of the 6s AO of gold because of the relativistic effects.

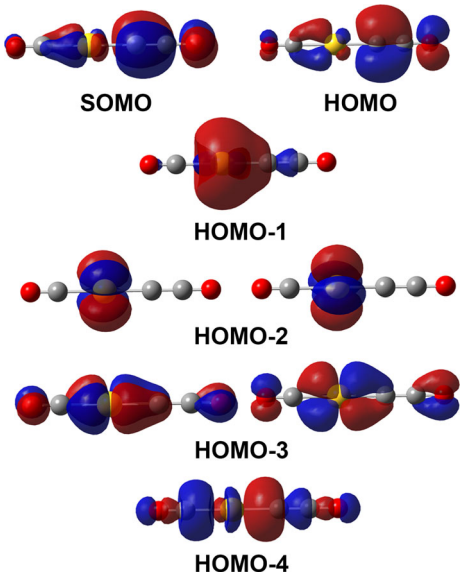

FIGURE 5 Shape of the highest-lying occupied molecular orbitals of OCTMCCO

3.6 | Reaction mechanism

The experimental observations clearly indicate that the ground state coinage metal atoms react with the C_3O_2 molecule in forming the TM-η^1-C_3O_2 complexes spontaneously on annealing in solid neon

TABLE 5 The EDA-NOCV results of OCTMCCO at the PBE/TZ2P//B3LYP/aug-cc-pVTZ level using the TM^+ (^1S) and $[OC...CCO]^-$ ($^2\Pi$) as interacting fragments. Energy values are given in kcal mol^{-1}

Energy	Assignment	(^1S) Cu^+ + ($^2\Pi$) $[OC...CCO]^-$	(^1S) Ag^+ + ($^2\Pi$) $[OC...CCO]^-$	(^1S) Au^+ + ($^2\Pi$) $[OC...CCO]^-$
ΔE_{int}	\	−263.0	−227.6	−293.1
ΔE_{pauli}	\	217.8	241.7	378.7
ΔE_{elstat}[a]	\	−343.2 (71.4%)	−346.1 (73.7%)	−466.7 (69.5%)
ΔE_{orb}[a]	\	−137.6 (28.6%)	−123.2 (26.3%)	−205.1 (30.5%)
$\Delta E_{orb\ (1)}$[b]	$[OC...CCO]^- \rightarrow [TM]^+$ σ donation (+, +)	−40.9 (29.7%)	−47.5 (38.6%)	−94.0 (45.8%)
$\Delta E_{orb\ (2)}$[b]	$[OC...CCO]^- \rightarrow [TM]^+$ σ donation (+, −)	−32.7 (23.8%)	−25.8 (20.9%)	−28.5 (13.9%)
$\Delta E_{orb\ (3)}$[b]	$[TM]^+ \rightarrow [OC...CCO]^-$ $\pi_{||}$-back donation	−22.0 (16.0%)	−16.7 (13.5%)	−26.2 (12.8%)
$\Delta E_{orb\ (4)}$[b]	$[TM]^+ \rightarrow [OC...CCO]^-$ $\pi_{\perp}$-back donation	−20.2 (14.7%)	−14.0 (11.4%)	−23.1 (11.3%)
$\Delta E_{orb(rest)}$	\	−21.8 (15.8%)	−19.2 (15.6%)	−33.3 (16.2%)

[a]The values in the parentheses show the contribution to the total attractive interaction ΔE_{elstat} plus ΔE_{orb}.
[b]The values in the parentheses show the contribution to the total orbital interaction ΔE_{orb}.

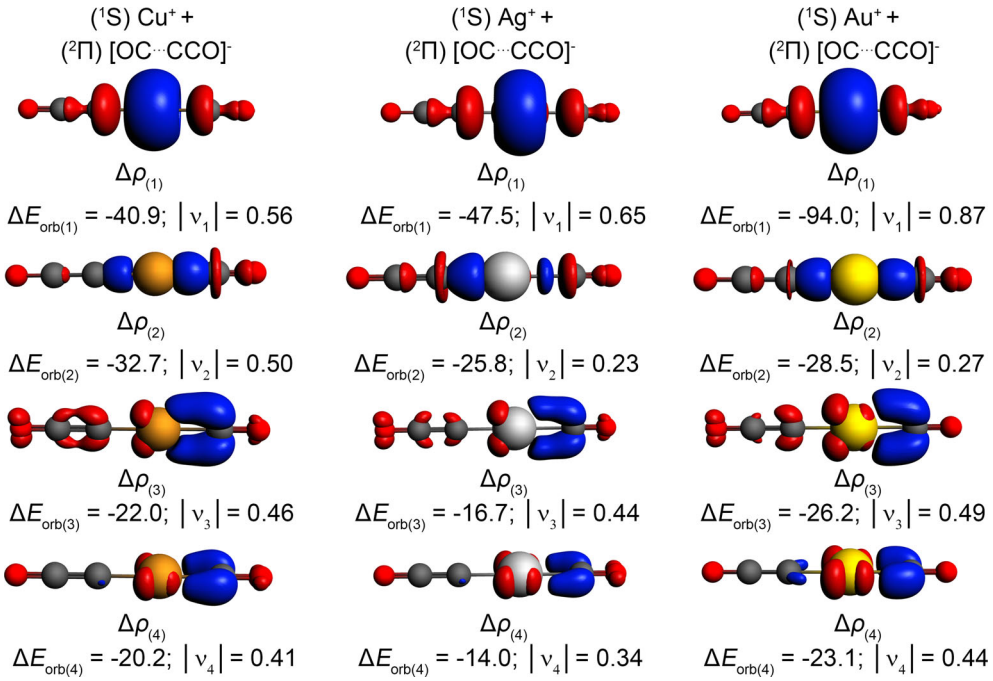

FIGURE 6 Plot of the deformation densities $\Delta\rho_{(1)-(4)}$, which are associated with the orbital interactions $\Delta E_{orb(1)-(4)}$ in OCTMCCO. The isosurface values are 0.003 a.u. for $\Delta\rho$ and 0.05 a.u. for orbitals. The charge flow of the deformation densities is red → blue

matrix. These addition reactions are predicted to be exothermic by 6.9 (Cu), 1.0 (Ag), and 6.8 kcal mol^{-1} (Au), respectively. The TM-η^1-C_3O_2 complexes can further isomerize to the linear inserted OCTMCCO isomers under visible light excitation. These isomerization reactions are predicted to be exothermic by 3.6 kcal mol^{-1} for Cu, but endothermic by 16.8 and 0.3 kcal mol^{-1} for Ag and Au, respectively. Theoretical calculations predict that the isomerization reaction for Cu in the ground state potential energy surface proceeds via a transition state lying 40.6 kcal mol^{-1} above the Cu-η^1-C_3O_2 complex (Figure S14). The reaction proceeds only under visible light irradiation with the photon energy sufficient to overcome the barrier. The isomerization reaction is a photo-induced process in which some excited states might be involved.

Besides the OCTMCCO complexes, the TMCCO complexes are also formed in the experiments. The TMCCO absorptions are observed on sample deposition and decrease on annealing, but slightly increase on blue light irradiation. It is assumed that the TMCCO complexes are formed from decomposition of the OCTMCCO complexes upon sample deposition or upon blue light irradiation. The decomposition reactions OCTMCCO → TMCCO + CO are predicted to be endothermic by 35.4, 25.2 and 40.1 kcal mol^{-1}, respectively.

4 | CONCLUSIONS

Matrix isolation infrared spectroscopy studies on the reactions of coinage metal atoms (Cu, Ag, and Au) with carbon suboxide show that the ground state metal atoms react with carbon suboxide to form the weakly bound TM-η^1-C_3O_2 complexes spontaneously on annealing in solid neon. The TM-η^1-C_3O_2 complexes further isomerize to the metal inserted ketenylidene complexes OCTMCCO under blue light irradiation. The OCTMCCO complexes are predicted to be linear. The TMCCO complexes are also formed, which are predicted to be bent. Bonding analysis indicates that the OCTMCCO complexes are best described by the bonding interactions between a TM^+ cation in the electronic singlet ground state ^1S and the $[OC...CCO]^-$ ligands in the doublet state with the unpaired electron in the π orbital of CCO^-. The attractive metal–ligand interactions in all these complexes come mainly from Coulomb attraction. The covalent orbital interactions are dominated by the TM^+ ← ligands σ donation and TM^+ → ligands π backdonation bonding components.

ACKNOWLEDGMENTS

The authors gratefully acknowledge financial support from the National Natural Science Foundation of China (Grant No. 21688102) and China Postdoctoral Science Foundation (No. 2020M681148).

DATA AVAILABILITY STATEMENT

The data that support the findings of this study are available in the supplementary material of this article and from the corresponding author upon reasonable request.

ORCID

Mingfei Zhou https://orcid.org/0000-0002-1915-6203

REFERENCES

[1] D. A. Long, F. S. Murfin, R. L. Williams, *Proc. R. Soc. London, Ser. A* **1954**, *223*, 251.
[2] R. L. Livingston, C. N. R. Rao, *J. Am. Chem. Soc.* **1959**, *81*, 285.
[3] F. A. Miller, W. G. Fateley, *Spectro. Chim. Acta.* **1964**, *20*, 253.
[4] M. Tanimoto, K. Kuchitsu, Y. Morino, *Bull. Chem. Soc. Jpn.* **1970**, *43*, 2776.
[5] L. A. Carreira, R. O. Carter, J. R. Durig, R. C. Lord, C. C. Milionis, *J. Chem. Phys.* **1973**, *59*, 1028.

[6] P. R. Bunker, *J. Mol. Spectrosc.* **1980**, *80*, 422.
[7] P. Jensen, J. W. C. Johns, *J. Mol. Spectrosc.* **1986**, *118*, 248.
[8] J. Vander Auwera, J. W. C. Johns, O. L. Polyansky, *J. Chem. Phys.* **1991**, *95*, 2299.
[9] J. Koput, *Chem. Phys. Lett.* **2000**, *320*, 237.
[10] R. Tonner, G. Frenking, *Chem. – Eur. J.* **2008**, *14*, 3260.
[11] G. Frenking, *Angew. Chem., Int. Ed.* **2014**, *53*, 6040.
[12] R. Tonner, G. Frenking, *Chem. – Eur. J.* **2008**, *14*, 3273.
[13] R. Tonner, G. Heydenrych, G. Frenking, *ChemPhysChem* **2008**, *9*, 1474.
[14] J. Tortajada, G. Provot, J. P. Morizur, J. F. Gal, P. C. Maria, R. Flammang, Y. Govaert, *J. Mass Spectrom.* **1995**, *141*, 241.
[15] J. Y. Jin, L. L. Zhao, X. N. Wu, W. Li, Y. H. Liu, D. M. Andrada, M. F. Zhou, G. Frenking, *J. Phys. Chem. A* **2017**, *121*, 2903.
[16] H. Nonaka, M. Uematsu, K. Yamanouchi, T. Kondow, K. Kuchitsu, *Chem. Phys.* **1989**, *133*, 165.
[17] L. N. Wang, S. Pan, B. Lu, X. L. Dong, H. M. Li, G. H. Deng, X. Q. Zeng, M. F. Zhou, G. Frenking, *Angew. Chem., Int. Ed.* **2021**, *60*, 4518.
[18] T. Kappe, E. Ziegler, *Angew. Chem., Int. Ed. Engl.* **1974**, *13*, 491.
[19] G. Paiaro, L. Pandolfo, *Angew. Chem., Int. Ed.* **1981**, *20*, 288.
[20] L. Pandolfo, F. Morandini, G. Paiaro, *Gazz. Chim. Ital.* **1985**, *115*, 711.
[21] A. K. List, M. R. Smith III., G. L. Hillhouse, *Organometallics* **1991**, *10*, 361.
[22] M. Casarin, L. Pandolfo, A. Sassi, *Organometallics* **2002**, *21*, 2235.
[23] Z. Zhang, L. Pu, X. Zhao, Q. S. Li, R. B. King, *New J. Chem.* **2016**, *40*, 9486.
[24] C. Esterhuysen, G. Frenking, *Chem. – Eur. J.* **2011**, *17*, 9944.
[25] H. Qu, G. J. Wang, M. F. Zhou, *J. Phys. Chem. A* **1978**, *2016*, 120.
[26] N. Tsoureas, J. C. Green, F. G. N. Cloke, H. Puschmann, S. M. Roea, G. Tizzard, *Chem. Sci.* **2018**, *9*, 5008.
[27] N. Tsoureas, F. G. N. Cloke, *Chem. Commun.* **2018**, *54*, 8830.
[28] G. J. Wang, M. F. Zhou, *Int. Rev. Phys. Chem.* **2008**, *27*, 1.
[29] B. Lu, C. Song, W. Y. Qian, Z. Wu, A. G. Császár, X. Q. Zeng, *Chem. Commun.* **2019**, *55*, 13510.
[30] M. J. Frisch, G. W. Trucks, H. B. Schlegel, G. E. Scuseria, M. A. Robb, J. R. Cheeseman, G. Scalmani, V. Barone, B. Mennucci, G. A. Petersson, et al., *Gaussian 09, revision A02*, Gaussian, Inc, Wallingford, CT **2009**.
[31] A. D. Becke, *Phys. Rev. A* **1988**, *38*, 3098.
[32] C. T. Lee, W. T. Yang, R. G. Parr, *Phys. Rev. B: Condens. Matter* **1988**, *37*, 785.
[33] A. D. Becke, *J. Chem. Phys.* **1993**, *98*, 5648.
[34] R. A. Kendall, T. H. Dunning, R. J. Harrison, *J. Chem. Phys.* **1992**, *96*, 6796.
[35] D. Andrae, U. Häußermann, M. Dolg, H. Stoll, H. Preuß, *Theor. Chim. Acta* **1990**, *77*, 123.
[36] S. Grimme, J. Antony, S. Ehrlich, H. Krieg, *J. Chem. Phys.* **2010**, *132*, 154104.
[37] T. Ziegler, A. Rauk, *Theor. Chim. Acta* **1977**, *46*, 1.
[38] M. Mitoraj, A. Michalak, *Organometallics* **2007**, *26*, 6576.
[39] E. van Lenthe, E. J. Baerends, *J. Comput. Chem.* **2003**, *24*, 1142.
[40] ADF, *SCM, Theoretical Chemistry*, Vrije Universiteit, Amsterdam, The Netherlands **2014** http://www.scm.com
[41] G. Te Velde, F. M. Bickelhaupt, E. J. Baerends, C. F. Guerra, S. J. A. van Gisbergen, J. G. Snijders, T. Ziegler, *J. Comput. Chem.* **2001**, *22*, 931.
[42] M. E. Jacox, D. E. Milligan, N. G. Moll, W. E. Thompson, *J. Chem. Phys.* **1965**, *43*, 3734.
[43] M. F. Zhou, L. Andrews, *J. Chem. Phys.* **1999**, *111*, 4548.
[44] E. T. Blues, D. Bryce-Smith, R. Shaoul, H. Hirsch, M. J. Simons, *J. Chem. Soc. Perkin Trans* **1993**, *9*, 1631.
[45] P. Pyykkö, M. Atsumi, *Chem. – Eur. J.* **2009**, *15*, 186.
[46] B. Y. Liang, L. Andrews, *J. Phys. Chem. A* **2000**, *104*, 9156.
[47] M. F. Zhou, L. Andrew, C. W. Bauschlicher, *Chem. Rev.* **2001**, *101*, 1931.
[48] P. H. Kasai, P. M. Jones, *J. Am. Chem. Soc.* **1985**, *107*, 6385.
[49] P. H. Kasai, P. M. Jones, *J. Phys. Chem.* **1985**, *89*, 1147.
[50] P. Pyykkö, M. Atsumi, *Chem. – Eur. J.* **2009**, *15*, 12770.
[51] D. Y. Zubarev, A. I. Boldyrev, *Phys. Chem. Chem. Phys.* **2008**, *10*, 5207.

SUPPORTING INFORMATION

Additional supporting information may be found in the online version of the article at the publisher's website.

How to cite this article: H. Li, Y. Zhou, G. Wang, X. Zeng, M. Zhou, *J. Comput. Chem.* **2023**, *44*(3), 129. https://doi.org/10.1002/jcc.26817